Hindawi
Journal of Advanced Transportation
Volume 2024, Article ID 4912642, 16 pages
https://doi.org/10.1155/2024/4912642

Research Article

Travel Time Reliability Estimation in Urban Road Networks: Utilization of Statistics Distribution and Tensor Decomposition

Linzhi Zou,[1] **Jiawen Wang**,[1] **Minqian Cheng**,[1] **and Jiayu Hang**[2]

[1]*Business School, University of Shanghai for Science and Technology, Shanghai 200093, China*
[2]*School of Urban Rail Transportation, Changzhou University, Changzhou 213164, Jiangsu, China*

Correspondence should be addressed to Jiawen Wang; wangjw@usst.edu.cn

Received 31 August 2023; Revised 3 April 2024; Accepted 10 April 2024; Published 23 April 2024

Academic Editor: Hui Bi

The travel time reliability (TTR) is crucial for evaluating the reliability of road networks, but real traffic data is often incomplete and sparse. This study validates that road network TTR conforms to a normal distribution and devises a quantification approach for road network TTR. Two reliability estimation methods are tailored for two data sources: section detectors and mobile detectors. Simulation experiments have confirmed the effectiveness of these methods. The study emphasizes that the TTR estimation method using traffic section data (S-TTR), which is based on the verified normal distribution assumption, maintains average absolute errors below 10%. On the other hand, the TTR estimation method that utilizes sparse trajectory data (T-TTR), which relies on tensor decomposition, proficiently fills in all missing data with an average error of 0.0059.

1. Introduction

To foster urban progress, it is crucial to improve transportation infrastructure and assess the status of road networks. Travel time reliability (TTR) is a critical metric for gauging the reliability of road networks [1]. Accurately estimating TTR for urban road networks and collecting reliable data can help transportation authorities optimize traffic networks [2–4].

Traffic data is crucial for TTR estimation on road networks, and the focus is now on data-driven solutions through Intelligent Transportation Systems [5]. By using real-time data, it is possible to estimate network conditions in real-time, which makes it easier to control the network dynamically [6]. Uneven deployment of data collection sensors can result in incomplete traffic data. Examples of such sensors include section detectors, floating vehicles, and satellite positioning. This leads to data gaps and losses, which can create a situation where the data used is substantial but sparse. The aim of this study is to estimate road network TTR using sparse data for accurate and reliable results.

This study proposes new methods for estimating road network TTR to enhance transportation efficiency. It utilizes traffic section detectors and trajectory data to offer customized estimation techniques for TTR. The contributions of this study are as follows:

(i) A method for measuring the reliability of urban road networks based on TTR has been proposed. Real data from the Huangpu District of Shanghai was used to verify that the network TTR follows a normal distribution. A numerical calculation method for TTR based on this pattern has also been proposed.

(ii) Two methods for estimating road network TTR have been introduced, using two different data sources. These methods are called the S-TTR (Travel Time Reliability of Network Based on Traffic Section Data) and T-TTR (Travel Time Reliability of Network Based on Sparse Trajectory Data) estimation methods.

(iii) Simulation experiments have validated the effectiveness of both S-TTR and T-TTR estimation methods. Additionally, the applicability of these methods has been demonstrated with data that has varying degrees of sparsity.

In the upcoming chapters, we have conducted a thorough examination of TTR. In Section 2, we have reviewed the literature on TTR. In Section 3, we have introduced a quantification method for TTR and have validated the normal distribution of TTR in the road network. We have proposed two estimation methods: S-TTR and T-TTR. In Section 4, we have comprehensively validated the effectiveness and applicability of both S-TTR and T-TTR estimation methods. Lastly, in Section 5, we have concluded this study by summarizing the aforementioned content and presenting our findings.

2. Literature Review

There are two methods to measure road network TTR: mathematical analytical methods and statistical measurement methods. The former uses traffic distribution models to calculate results, while the latter measures reliability by analyzing travel times. Mathematical methods can effectively consider various factors, but modeling and parameter calibration can be complex, limiting their use [7]. Traffic data collection devices now provide more accurate statistical measurements by collecting more data [8].

Due to the challenge of obtaining complete real-world traffic data, some studies use traffic simulation data to explore TTR. Khani and Boyles [9] found a solution for finding the most reliable path for risk-averse individuals by adding the mean and variance of route travel times. Researchers are now considering the differences between traffic simulation data and real-world data due to advancements in information technology. Taylor [10] utilized a three-parameter Burr distribution to fit travel time distribution and applied the Fosgerau method to estimate TTR. Li et al. [11] used the Lempel-Ziv algorithm from information theory to analyze TTR based on historical data.

Recent research is enhancing TTR estimation through traffic simulation and real-world data by incorporating origin-destination data and simplifying network models for better accuracy and efficiency. The data-driven methods used in this study can provide a more accurate depiction of actual road network conditions.

Traffic data is collected using section detectors to gather information on flow, occupancy, and speed. However, these cannot provide travel time data directly. The lack of section detectors in some links and the absence of positioning devices in some vehicles leads to data sparsity, making current traffic flow prediction methods ineffective. These methods require raw data input and training processes such as time-series-based approaches and machine learning-related methods.

One effective solution for handling data sparsity is constructing models, such as matrix and tensor factorization methods [12]. Tensor factorization is suitable for predicting historical missing data [13]. Tang et al. [14] constructed a three-dimensional tensor to simulate travel times for different links under varying traffic conditions during certain periods. The study considered the impact of congestion on travel times but lacked a comprehensive model analysis. Zhong et al. [15] employed tensor factorization to identify traffic patterns. Pastor [16] proposed a low-rank tensor model for handling vehicle traffic volume data, utilizing the correlation between local structures present in multiple models and enhancing tensor sequence rank accuracy by optimizing balanced tensors. Additionally, Tan et al. [17] introduced a tensor-based approach to model and complete missing traffic data values.

This study proposes a new method to estimate TTR in road networks using the Bureau of Public Roads (BPR) function. A threshold is determined based on traffic section data to introduce a TTR estimation method. Additionally, a tensor-based TTR estimation method using decomposition is proposed to overcome sparsity in trajectory data.

3. Methodology

3.1. Notation. The relevant parameters in this study are listed in Table 1.

3.2. Hypothesis and Validation. The delay travel time ratio measures the ratio of the total delay incurred by an individual vehicle during its journey within a road network to the total travel time. We analyzed traffic network and trajectory data collected in Huangpu, Shanghai, China, between May 25 and May 31, 2020, with 29,785 links and 94,658,941 trajectories. Based on our analysis, we determined that the delay travel time ratios of vehicles in the road network follow a normal distribution, as depicted in Figures 1 and 2. Furthermore, a normal distribution fitting was applied to the probability distribution of delay travel time ratios, and the goodness of fit is presented in Table 2. The fitting results show that the distribution of delay travel time ratios for road network vehicles conforms to the characteristics of normal distribution.

Thus, the mathematical expression for the delayed travel time ratio of vehicles in the road network is

$$\frac{d}{t} = X \sim N\left(\mu, \sigma^2\right). \tag{1}$$

We define reliable travel as when the travel time of a single vehicle falls below or meets a predetermined threshold for its delay and travel time, otherwise it is considered unreliable. The corresponding reliability formula simplifies as $P(pc_m \le pc_0) = P(d/t \le pc_0)$. In accordance with definition and verified hypothesis, we conclude the TTR of the road network during dt as follows:

$$R(dt) = P\left(x \le pc_0\right) = \int_0^{pc_0} \frac{1}{\sqrt{2\pi}\sigma} \exp\left\{-\frac{(x-\mu)^2}{2\sigma^2}\right\} dx, \tag{2}$$

where μ represents the mean of the delay travel time ratio for vehicles in the road network, and σ^2 denotes the variance of the delay travel time ratio for vehicles in the road network.

According to the definition of the TTR of the road network, the ratio of the delay to the travel time of each vehicle passing through the road network is calculated according to the obtained vehicle trajectory data, and the

Table 1: Parameter description.

Parameter	Description	Unit
dt:	Length of time window	s
T:	Total time range for reliability analysis, as the sum of the time windows	s
$\widetilde{N}_a(dt)$:	Total number of vehicles traveling in link a during dt	pcu
$\widetilde{N}(dt)$:	Total number of vehicles traveling on the road network during dt	pcu
$\widetilde{q}_a(dt)$:	Flow in link a during dt	pcu/h
L_a:	Length of link a	km
d_m:	Delays incurred by vehicle m from the time it enters the road network to the time it leaves the network	s/pcu
t_m:	Travel time of the vehicle m from entry to exit from the road network	s/pcu
pc_m:	Ratio of delayed travel time for vehicle m	—
pc_0:	Vehicle delay and travel time ratio threshold	—
$F(\bullet)$:	Probability that a trip is reliable for all vehicles on the road network	—
$P(\bullet)$:	Probability that the ratio of delayed travel times for all vehicles on the road network is less than a reliability threshold	—
R:	TTR of road networks	—
$n(\bullet)$:	Number of vehicles with reliable trips out of the total number of vehicles leaving the network at a given time	pcu
$N(\bullet)$:	Total number of vehicles leaving the road network at a given time	pcu
x_a:	Traffic volume of link a	pcu
$t_a(x_a)$:	The travel time of link a, when the traffic volume of link a is x_a	s
t_a^0:	Free-flow travel time of link a	s
C_a:	Capacity of link a	pcu/h
α, β:	Measured calibration parameters by travel time in links of the same class	—
ω, θ:	Model parameters	—
s_l:	Turn correction factor	—
g_s:	Downstream phase green ratio	—
$d_a(x_a)$:	The delay of link a, when the traffic volume of link a is x_a	s
TTD (TTS):	The actual value of the total distance traveled by the vehicle for the corresponding travel time	m
$\overline{\text{TTD (TTS)}}$:	Desired value of the total distance traveled by the vehicle for the corresponding travel time	m
δ:	Estimated coefficient of variance	—
$\underset{\sim}{\mathbf{x}}$:	Tensor with missing data, $\mathbf{x} \in \mathbb{R}^{I_1 \times I_2 \times \cdots \times I_N}$	—
$\widehat{\mathbf{x}}$:	Estimate of $\mathbf{x}$	—
$\underset{\sim}{\mathbf{X}}$:	Sparse tensor of size $n_1 \times n_2 \times n_3$	—
$\widehat{\mathbf{X}}$:	Estimate of $\mathbf{X}$	—
$\mathbf{w}$:	Binary indicator tensor of the same dimension as $\mathbf{x}$	—
$\mathbf{A}^{(N)}$:	Factor matrices of tensor $\mathbf{x}$ on each mode	—
$\mathbf{a}_r^{(n)}$:	Column vector of index r of matrix $A^{(N)}$, $a_r^{(n)} \in \mathbb{R}^{I_n}$ and $A^{(N)} = [a_1^{(n)}, a_2^{(n)}, \cdots, a_R^{(n)}]$	—
$\sigma_i(\widehat{\mathbf{X}})$:	Singular value of index i of estimate matrix $\widehat{\mathbf{X}}$	—
$*$:	Hadamard product of tensors, also known as element-wise product	—
$\circ$:	Outer product of vectors	—
$\|\bullet\|$:	Norm of a tensor	—
$\|\bullet\|_*$:	Trace norm	—

probability distribution of the delay travel time ratio of the road network vehicles is shown in Figure 3.

For a certain vehicle m, the ratio of delay to travel time is pc_m. If $pc_m \le pc_0$, the trip of vehicle m is considered reliable; If $pc_m > pc_0$, it is considered that the trip of vehicle m is unreliable. Hence, the reliability of the dynamic road network is meant to quantify the likelihood of all vehicles traversing the road network successfully within T time under specific conditions. The integral formulation of this reliability is displayed in equation (3), whilst its discrete counterpart can be seen in equation (4).

$$R(T) = F(pc_m = pc_0) = P(pc_m \le pc_0) = \int_0^T \frac{n(t)}{N(t)} dt, \tag{3}$$

$$\mathrm{R}(T) = \frac{n(t)}{N(t)}. \tag{4}$$

Increased $R(T)$ lead to more reliable travel times for vehicles, enhancing network reliability. Thus, TTR can be expressed as a normal distribution ratio of delay to travel time during a time period dt.

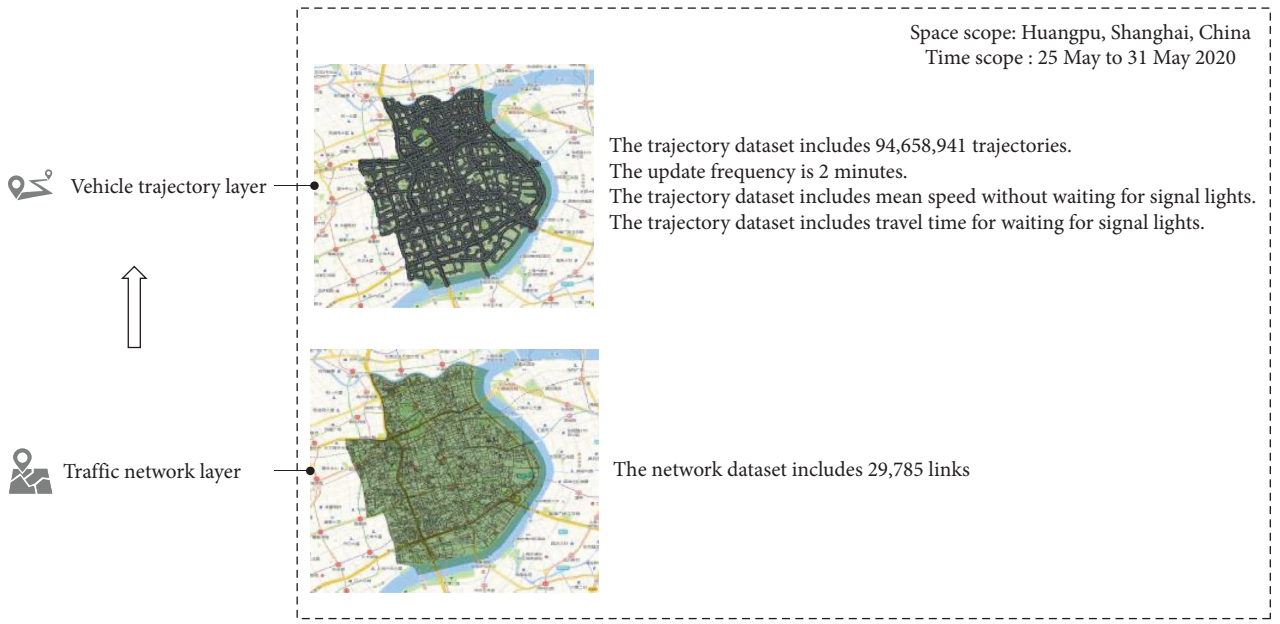

Figure 1: Schematic diagram of traffic network and trajectory data collected in Huangpu, Shanghai, China, from May 25 to May 31, 2020.

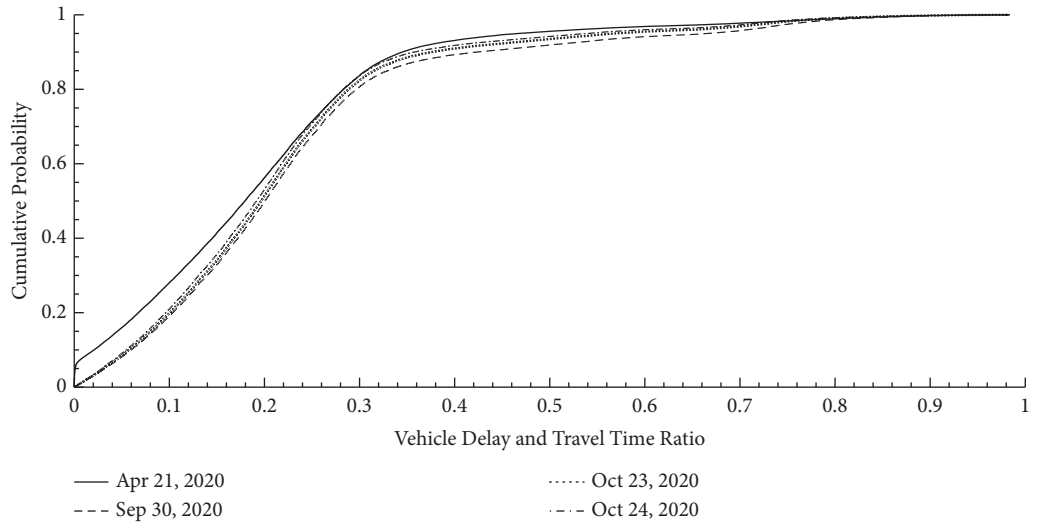

Figure 2: Cumulative probability distribution of vehicle delay and travel time ratio in four natural days.

Table 2: Distribution goodness of fit of delay and travel time ratio.

	April 21	September 30	October 23	October 24
Logarithm of a distribution		Normal		
Likelihood function value	$1.22E+06$	$1.06E+06$	$1.27E+06$	$1.36E+06$
Range	-Inf < y < Inf	-Inf < y < Inf	-Inf < y < Inf	-Inf < y < Inf
Mean value	0.1956	0.2297	0.2194	0.2123
Variance	0.0239	0.0289	0.0249	0.0233

Equation (4) calculates real-time reliability for the road network determined within a specific time span instead of integrating over the entire temporal scale.

3.3. Reliability Estimation Method. The threshold pc_0 is determined by referencing the percentile of the delay travel time ratio probability distribution. Given that the population

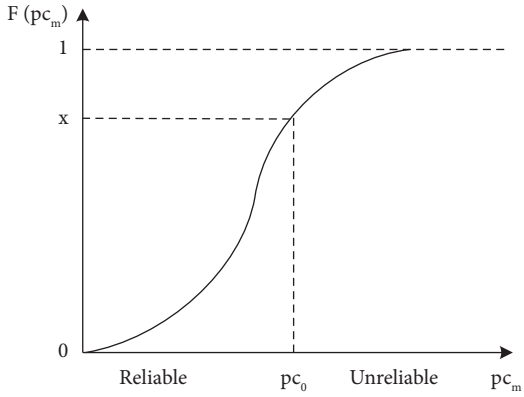

Figure 3: Quantification curve of TTR of dynamic road network.

follows a normal distribution $X \sim N(\mu, \sigma^2)$, for a given value of $\omega\,(0 < \omega \leq 1)$, if there exists x_ω such that $P\{X \geq x_\omega\} = \omega$, then $pc_0 = x_\omega$.

For urban road networks, research indicates that travel times increase monotonically with traffic demand and exhibit a convex function, consistent with the BPR function [18]. Zhao et al. [19] formulated a BPR correction model for urban road networks based on the BPR model, applicable for networks with signalized intersections and conditions close to traffic capacity saturation. Within the same time interval dt, the delay for link a is given by

$$d_a(x_a) = t_a(x_a) - t_a^0 = \alpha \cdot t_a^0 \cdot \left(\frac{x_a}{c_a}\right)^\beta, \tag{5}$$

where $t_a(x_a) = t_a^0[1 + \alpha(x_a/c_a)^\beta]$ and $\alpha = \omega(1 - s_l) + \theta \cdot g_s$. Consequently, the delay travel time ratio for the entire road network U within a specific time period is given by

$$\mu = \frac{\sum_{u=a}^{n} d_u(x_u)}{\sum_{u=a}^{n} t_u(x_u)}, \quad u = a, b, c \ldots \in U. \tag{6}$$

The estimation of the variance σ^2 of the road network vehicle delay travel time is the focus and difficulty of this study. To assess the variance σ^2 of the delay travel time ratio distribution, we need to analyze the unevenness of travel time per unit distance on the road network. Network density distribution is studied about the macroscopic fundamental diagram discreteness [1, 20, 21]. Knoop et al. [21] proposed the theory of the generalized macroscopic fundamental diagram, emphasizing the correlation between road network performance (i.e., total travel distance (TTD) in this study), cumulative vehicles in the network (i.e., total time spent (TTS) in this study), and the unevenness of link vehicle density. Based on this research, this study employs the difference between the ideal value of $\overline{\mathrm{TTD}}(\mathrm{TTS})$ with completely uniform network density and the TTD of vehicles detected in real-time $\mathrm{TTD}(t)$ as input parameters for estimating the variance σ^2 of the delay travel time ratio distribution.

Figure 4 illustrates the variance estimation method. The ideal value is situated on the envelope of the macroscopic fundamental diagram, as demonstrated by the dotted box in the figure, demonstrating the correlation between the difference and the evenness of the network density. The position of the point generated from the sum of the TTD and the number of vehicles can be found below the envelope when the road network encounters unexpected events like traffic accidents. The study assumes that when the vehicle density and expectations of the road network remain constant, scatter points inclined upward indicate higher reliability with higher TTD and smaller variance, while those inclined downward signify decreased reliability and increased variance. Therefore, a variance estimation method is established accordingly.

Through section detection, the TTD and number of vehicles on a network can be estimated, including their dynamics curve and related point positioning at different moments [22]. Notably, the normal curve for the TTD and number of vehicles in an homogeneous network accounts for signal control within the road network [23]. Real-time methods to predict TTD and TTS are as follows:

$$\mathrm{TTS}(dt) = \sum_{a \in U} \frac{T \cdot \widehat{N_a}(dt)}{T} = \sum_{a \in U} \widehat{N_a}(dt) = \widehat{N}(dt), \tag{7}$$

$$\mathrm{TTD}(dt) = \sum_{a \in U} \frac{T \cdot \widehat{q_a}(dt) \cdot L_a}{T} = \sum_{a \in U} \widehat{q_a}(dt) \cdot L_a. \tag{8}$$

Due to network configuration, signaling, organization, and incidents, traffic lane inequality leads to network heterogeneity. This could render an equilibrium curve for the TTD and total vehicle count, despite homogeneous network conditions [23]. However, under such non-homogeneous network conditions, a definite relationship still exists between the two parameters. The actual value of the $\mathrm{TTD}(\mathrm{TTS})$ may deviate from the ideal value $\overline{\mathrm{TTD}(\mathrm{TTS})}$. The extent of deviation signifies the stability of TTR in the road network to some degree; greater deviation suggests increased instability in TTR and a larger variance in the delay travel time ratio. In practice, the TTD will not exceed the idealized $\overline{\mathrm{TTD}}$. If $\mathrm{TTD} = \overline{\mathrm{TTD}}$, it signifies uniform vehicle density in the road network. Under such conditions, travel times per unit distance are entirely equal, leading to a variance of the delay travel time ratio of 0. Consequently, in the linear estimation model for variance, the constant term should be 0. In this study, the difference between TTD and $\overline{\mathrm{TTD}}$ is 0, rendering the output of the variance estimation accurate, i.e., 0. Hence, the linear estimation model for variance does not possess a constant term. In the ideal state, the real-time estimation method for σ^2 is expressed as follows:

$$\sigma^2 = \delta|\mathrm{TTD}(\mathrm{TTS}) - \overline{\mathrm{TTD}(\mathrm{TTS})}|, \tag{9}$$

where δ is the coefficient for variance estimation. In practical applications, it will be calibrated using sampled data from three traffic states: (i) under ideal free-flow conditions, (ii) under reliable critical conditions, and (iii) under unreliable congestion conditions, denoted as δ_f, δ_s, and δ_j, respectively.

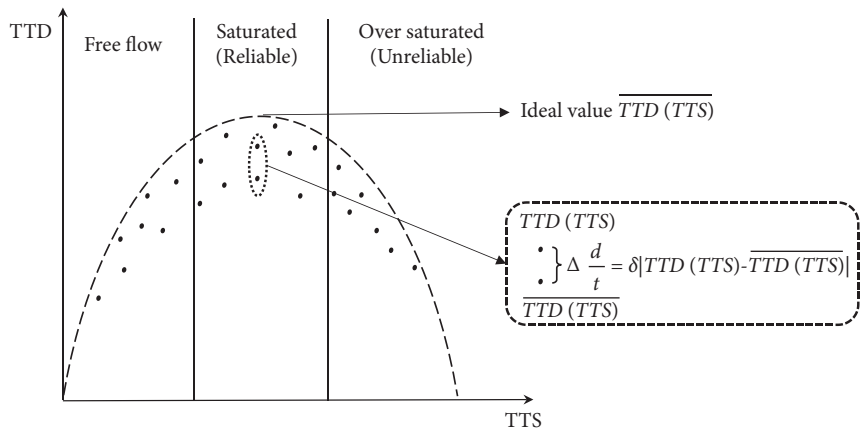

Figure 4: Schematic diagram of variance estimation.

3.3.1. S-TTR Estimation Method. The utilization of the BPR function yields the expected value μ of the delay travel time ratio for vehicles in the road network. From the equilibrium curve of the TTD and the total number of vehicles, a linear estimation model for the variance σ^2 of the delay travel time ratio is introduced. This model is illustrated in equations (6) and (9). In both equations, it is necessary to determine the flow $\widehat{q_a}(dt)$ on links during the interval dt, the total number of vehicles $\widehat{N_a}(dt)$ traveling on each link, and the total number of vehicles $\widehat{N}(dt)$ on the road network U. Section detectors facilitate the dynamic acquisition of these pertinent parameters. This acquisition subsequently enables the calculation of the expected value μ and variance σ^2 for the delay travel time ratio of road network vehicles. The workflow of the S-TTR estimation method is illustrated in Figure 5.

3.3.2. T-TTR Estimation Method. In this subsection, we present a method for estimating TTR across an entire urban road network using sparse trajectory data. Urban road networks are complex, with traffic demand and supply imbalances between regions and variations in reliability at different times. Consequently, TTR displays both spatial and temporal unevenness. Our approach designs a third-order tensor defining the network's x-axis regions, y-axis regions, and time intervals. Leveraging temporal correlation of data, missing elements in spatial region tensors can be filled via a context-aware tensor methodology. The method not only considers the spatial correlation of TTR among neighboring regions but also acknowledges the temporal correlation of TTR over different time intervals. For an Nth-order tensor $\mathbf{x} \in \mathbb{R}^{I_1 \times I_2 \times \cdots \times I_N}$ with missing data, the optimization objective function for tensor completion employing canonical polyadic decomposition is established as follows:

$$\min f_w\left(\mathbf{A}^{(1)}, \mathbf{A}^{(2)}, \cdots, \mathbf{A}^{(\mathrm{N})}\right) = \frac{1}{2}\left\|\mathbf{w} * \left(\mathbf{x} - [\![\mathbf{A}^{(1)}, \mathbf{A}^{(2)}, \cdots, \mathbf{A}^{(\mathrm{N})}]\!]\right)\right\|^2, \tag{10}$$

$$[\![\mathbf{A}^{(1)}, \mathbf{A}^{(2)}, \cdots, \mathbf{A}^{(N)}]\!] = \sum_{r=1}^{R} \mathbf{a}_r^{(1)} \circ \mathbf{a}_r^{(2)} \circ \cdots \circ \mathbf{a}_r^{(N)}. \tag{11}$$

For all $i_n \in \{1, 2, \cdots, I_n\}$ and $n \in \{1, 2, \cdots, N\}$, $\mathbf{w}$ defined as follows:

$$w_{i_1 i_2 \cdots i_N} = \begin{cases} 1 & \text{if } x_{i_1 i_2 \cdots i_N} \text{ is known,} \\ 0 & \text{if } x_{i_1 i_2 \cdots i_N} \text{ is missing.} \end{cases} \tag{12}$$

If the optimal factor matrices calculated from equation (10) are denoted as $\overline{\mathbf{A}}^{(1)}, \overline{\mathbf{A}}^{(2)}, \cdots, \overline{\mathbf{A}}^{(N)}$, the missing data of the original tensor x can be estimated using the following equation:

$$(\mathbf{1} - \mathbf{w}) * [\![\overline{\mathbf{A}}^{(1)}, \overline{\mathbf{A}}^{(2)}, \cdots, \overline{\mathbf{A}}^{(\mathrm{N})}]\!]. \tag{13}$$

Based on this, the complete form of the original tensor $\mathbf{x}$ can be computed using the following equation:

$$\mathbf{x}_{\mathrm{rec}} = \mathbf{w} * \mathbf{x} + (\mathbf{1} - \mathbf{w}) * [\![\mathbf{A}^{(1)}, \mathbf{A}^{(2)}, \cdots, \mathbf{A}^{(\mathrm{N})}]\!], \tag{14}$$

where the first part corresponds to the known data in the original tensor, while the second part represents the estimated values for the missing data in the original tensor.

To accurately estimate the TTR on a road network, missing data can be filled in using tensor completion theory. This involves using a specific algorithm called high accuracy low-rank tensor completion (HaLRTC) [24] to impute the missing data. The concept of tensors is introduced in this subsection, and a new approach to modeling TTR called the T-TTR estimation method is proposed by integrating the HaLRTC algorithm.

Given a sparse tensor $\mathbf{X}$ of size $n_1 \times n_2 \times n_3$ (sparse due to missing entries), with the indices corresponding to observed elements denoted as $(i, j, k) \in \Omega$, a tensor $\mathbf{S}$ of the same size

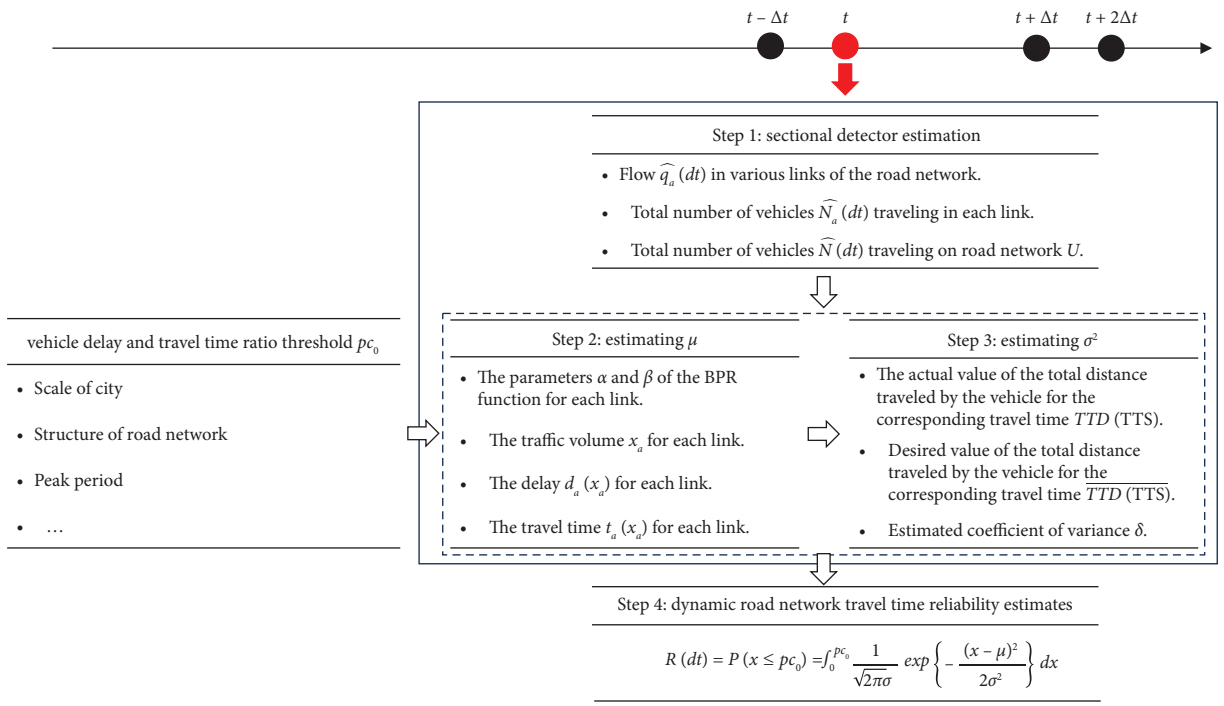

Figure 5: The production of road network TTR estimated by section detection data.

is defined as a binary tensor consisting of elements 0 and 1. Specifically, $S_{ij} = 1$, $(i, j) \in \Omega$, otherwise $S_{ij} = 0$, $(i, j) \notin \Omega$. The objective function of tensor completion problem can be formulated as follows:

$$\min_{\widehat{\chi}, B_1, B_2, B_3} \alpha_1 \left\| B_{1(1)} \right\|_* + \alpha_2 \left\| B_{2(2)} \right\|_* + \alpha_3 \left\| B_{3(3)} \right\|_* \quad (15)$$

where the tensors $\mathbf{B}_1$, $\mathbf{B}_2$, and $\mathbf{B}_3$ are all of size $n_1 \times n_2 \times n_3$. The matrix $\mathbf{B}_{1(1)}$ of size $n_1 \times (n_2 n_3)$ represents the unfolding of tensor $\mathbf{B}_1$ in mode 1. Similarly, the matrix $\mathbf{B}_{2(2)}$ represents the unfolding of $\mathbf{B}_2$ in mode 2, and the matrix $\mathbf{B}_{3(3)}$ represents the unfolding of $\mathbf{B}_3$ in mode 3.

The optimization model has two constraints: the first one ensures that the estimated tensor $\widehat{\mathbf{x}}$ and the original tensor $\mathbf{x}$ have equal elements over the set Ω; the second one sets the intermediate variables $\mathbf{B}_1$, $\mathbf{B}_2$ and $\mathbf{B}_3$ equal to the estimated tensor $\widehat{\mathbf{x}}$. The specifics are as follows:

$$s.t. \begin{cases} S * \widehat{X} = S * X, \\ \widehat{X} = B_q, \quad q = 1, 2, 3. \end{cases} \quad (16)$$

In the objective function, the parameters α_1, α_2, and α_3 need to satisfy the condition: $\alpha_1 + \alpha_2 + \alpha_3 = 1$. Typically, setting $\alpha_1 = \alpha_2 = \alpha_3 = 1/3$ is sufficient.

The aforementioned model yields the reliability estimate $\widehat{\mathbf{X}}_i$ for region i. Due to the nonuniform distribution of data in road network regions, some regions have a small amount of data or even lack data. To address this, a variable a is introduced, which is related to penetration rate, time window length, and traffic flow. When the data quantity θ_i in road network region i is less than or equal to a, the data for that region is treated as missing (assumed to be $\mathbf{0}$), as outlined:

$$\widehat{\mathbf{X}}_i = \begin{cases} \widehat{\mathbf{X}}_i \, if \, \theta_i > a \\ \mathbf{0} \, if \, \theta_i \le a \end{cases}, a = \theta_\beta, \theta = \theta_1 + \theta_2 + \cdots + \theta_i. \quad (17)$$

Due to the temporal correlation present in the TTR data of road network, an exponential smoothing method is introduced to update the aforementioned model. This further enhances the influence of known data within the time window on estimated data. The fundamental formula for exponential smoothing is as follows:

$$\mathbf{S}_t = a \cdot \mathbf{y}_t + (1 - a)\mathbf{S}_{t-1}, \quad (18)$$

where $\mathbf{S}_t$ represents the smoothed value at time t, $\mathbf{y}_t$ represents the actual value at time t, and a is the smoothing constant, ranging between 0 and 1. The model update formula is as follows:

$$\widehat{\mathbf{X}}_i = \begin{cases} \widehat{\mathbf{X}}_i \, if \, \theta_i > a, \\ \\ \frac{\gamma}{i} \cdot \mathbf{X}_i + \left(1 - \frac{\gamma}{i}\right) \cdot \mathbf{S}_{\widehat{\mathbf{X}}_i} \, if \, \theta_i \le a, \end{cases} \quad (19)$$

where γ represents the number of road network regions with the least amount of data, and $\mathbf{S}_{\widehat{\mathbf{X}}_i}$ denotes the estimate obtained through the updated exponential smoothing method.

The alternating direction method of multipliers (ADMM) is suitable for solving distributed convex optimization problems, known for its fast processing speed and good convergence properties. By leveraging the ADMM framework, we can derive iterative update formulas for tensors $\mathbf{B}_1$, $\mathbf{B}_2$, and $\mathbf{B}_3$, and the estimated tensor $\widehat{\mathbf{x}}$, thus obtaining the HaLRTC estimation method. Building upon the HaLRTC estimation method and combining it with the

T-TTR estimation method, the algorithm's specific workflow is as follows:

Step 1: Input: $\overrightarrow{\alpha} = (\alpha_1, \alpha_2, \alpha_3)$, ρ, and the maximum number of iterations K;

Step 2: Initialize the estimated tensor $\widehat{\mathbf{X}}$ such that $\widehat{\mathbf{x}_{ijk}} = \begin{cases} x_{ijk}, (i, j, k \in \Omega) \\ 0, (i, j, k \notin \Omega) \end{cases}$;

Step 3: Initialize additional variables $\mathbf{y}_1$, $\mathbf{y}_2$, and $\alpha\mathbf{y}_3 \in \mathbb{R}^{n_1 \times n_2 \times n_3}$ with all elements set to 0;

Step 4: Iteration, for $k = 1$:K do

Step 4.1: Update the tensor $\mathbf{B}_q$: $\mathbf{B}_q = \text{fold}_q\left\{D_{a_q/\rho}(\widehat{\mathbf{X}}_{(q)} + 1/\rho\mathbf{y}_{q(q)})\right\}, q = 1, 2, 3;$

Step 4.2: Update the estimated tensor $\widehat{\mathbf{X}}$: $\widehat{\mathbf{X}} = (\mathbf{1} - \mathbf{S}) * \left\{1/3 \sum_{q=1}^{3} (\mathbf{B}_q - 1/\rho\, \mathbf{y}_q)\right\} + \mathbf{S} * \mathbf{X};$

Step 4.3: Update the estimated tensor $\widehat{X}_i$ using missing data: if $\theta_i > a, \widehat{\mathbf{X}}_i = \widehat{\mathbf{X}}_i$; else $\widehat{\mathbf{X}}_i = \mathbf{0}, a = \theta_\beta$, $\theta = \theta_1 + \theta_2 + \cdots + \theta_i$;

Step 4.4: Update the estimated tensor $\widehat{\mathbf{X}}_i$ using exponential smoothing method: if $\theta_i > a, \widehat{\mathbf{X}}_i = \widehat{\mathbf{X}}_i$; else $\widehat{\mathbf{X}}_i = \gamma/i\mathbf{X}_i + (1 - \gamma/i)\, \mathbf{S}_{\widehat{\mathbf{X}}_i}$;

Step 4.5: Update the auxiliary variables $\mathbf{y}_q$: $\mathbf{y}_q = \mathbf{y}_q - \rho(\mathbf{B}_q - \widehat{\mathbf{X}}), q = 1, 2, 3;$

Step 5: Output $\widehat{\mathbf{X}}$.

In the algorithm, the operator $D_{a_q/\rho}(\cdot)$ is given a specific definition. Taking the example of a matrix $\mathbf{X}$ with dimensions $m \times n$ mentioned above, we have $D_{a_q/\rho}(\mathbf{X}) = \mathbf{U}\sum_{a_q/\rho}\mathbf{V}^T$, where $\sum_{a_q/\rho} = \text{diag}(\max(\sigma_i - a_q/\rho, 0))$; the symbol "$\text{fold}_q(\cdot)$" denotes the operation of reshaping a matrix back into a tensor, which is the reverse process of unfolding.

4. Simulation

4.1. Analysis of the Effectiveness of the S-TTR Method. This subsection utilized the VISSIM to test the effectiveness of the S-TTR estimation method. A case study was conducted on a 3×3 standard square microsimulation road network, as shown in Figure 6. The traffic composition, vehicle speed distribution, and car-following model parameters were calibrated using data from the Huangpu district of Shanghai, which has similar scale and road network conditions. The simulation road network had an intersection spacing of 500 meters, lane width of 3.5 meters, greenbelt width of 4 meters, and zebra crossing width of 8 meters. Each entrance lane consisted of two lanes, one for straight and left-turning vehicles and the other for straight and right-turning vehicles. The vehicle type used for the simulation was the "small car," each with an expected speed of 40 kilometers per hour, and their speeds follow a normal distribution in VISSIM. The intersections were two-phase signalized intersections with a signal cycle of 60 seconds, and the green light interval was set to 5 seconds.

Traffic flow is evenly distributed throughout the road network by assigning a fixed flow rate to each entrance lane and using a traffic assignment model. There are 25 input paths at the edge of the network and 21 in the middle, assuming that vehicles do not take detours. To achieve balance distribution, the road network is adjusted by removing four-turns and U-turn routes and adjusting traffic flows based on the number of turns. Straight movements are assigned a weight of 1, one-turn movements 0.5, two-turn movements 0.25, and three-turn movements 0.125.

We analyzed the impact of signal cycles on traffic network efficiency and reliability. Three scenarios were considered, with signal cycles of 60 s, 90 s, and 120 s at each intersection. A comparative analysis was conducted to assess the effectiveness of the S-TTR estimation method. The accuracy of the S-TTR method was evaluated by comparing the actual ground truth of network reliability (measured as the delay travel time ratio of each vehicle) using complete vehicle data to the estimated values obtained using the S-TTR method. This study analyzed simulation data to establish a threshold for delay travel time ratios within the network. Table 3 shows the percentage of the probability distribution for vehicle delay travel time ratios.

The graph in Figure 7 shows network reliability based on different delay travel time ratio thresholds. The pattern remains consistent for all thresholds, with a rapid drop in reliability shown by the solid line. The 75th percentile threshold, with a delay travel time ratio pc_0 of 0.6899, effectively represents the overall trend of reliability variation. This threshold was selected for the simulation.

We simulated various vehicle inputs and collected data for reliability estimation experiment calibration. Results are presented in Table 4. The relationship between reliability true values and estimated values is compared in Figure 8.

According to Figure 8(a), when the TTS initially increases, the traffic flow in the road network is smooth with no congestion. Both estimated and true reliability values are consistent and equal to 1. However, when the TTS exceeds a certain threshold, congestion starts to occur, and the traffic flow in the network approaches the critical flow state. In turn, both estimated and true reliability values start to decrease steadily. Nevertheless, the estimated values are higher than the true values, and the larger error region is in zone A. As the TTS continues to increase, traffic flow in the network becomes congested, causing significant delays for vehicles. This leads to a rapid decline in network reliability and unreliable travel times for vehicles, with delay ratios exceeding the threshold.

In Figure 8(b), there is a trend in the change in reliability values that is similar to Figure 8(c). The estimated values are slightly smaller than the true values, and there is a larger error region that is concentrated in zone B. Additionally, in Figure 8(c), the phenomenon of underestimation is even more evident, with a larger error region concentrated in zone C.

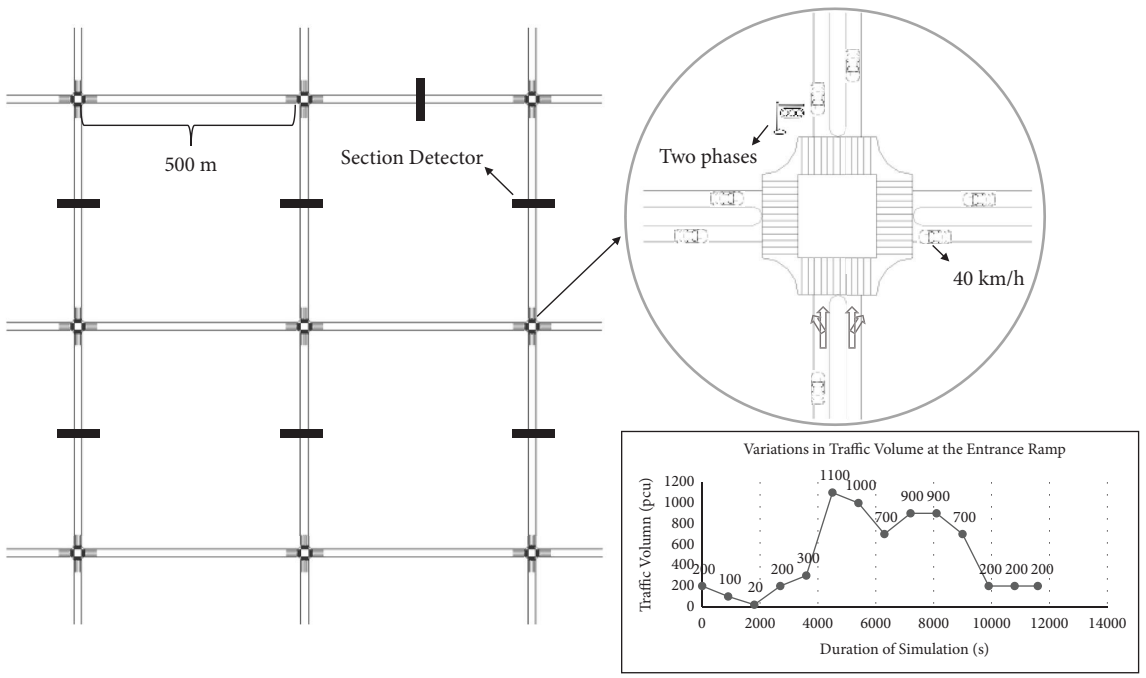

Figure 6: Diagram of simulation road network.

Table 3: Percentile of delayed travel time ratio probability distribution.

Percentile of the probability distribution of delayed travel time ratio (%)	Delayed travel time ratio
95	0.7674
85	0.7188
75	0.6899
65	0.6668
55	0.6461

Errors were found in the estimation method in zones A, B, and C when the road network was close to saturation. A comparison of true and estimated reliability values was conducted through 180-minute simulations with a 60-second statistical time window. Table 5 shows the results of the error analysis that used five different random seeds and averaged the findings.

Based on the above analysis results, it is clear that the S-TTR estimation method proposed in this study has an average absolute error of 0.0568, 0.0617, and 0.0759 for road network signal periods of the 60 s, 90 s, and 120 s respectively. These errors are all below 10%, indicating that the S-TTR estimation method can accurately estimate the reliability of the road network using data collected from section detectors.

4.2. Analysis of the Applicability of the S-TTR Method. This subsection aims to examine how different detector deployment strategies can affect the accuracy of road network TTR. Therefore, a regular 4 × 4 grid network is used as an example. Each intersection entrance has four lanes while the exit roads have three. Each lane measures 3.5 meters in length, and the total distance between any two intersections is 500 meters. The road network layout is based on these specifications. The network uses fixed-time signal control with four signal phases, each with its own set of signal lights. Phase 1 allows for an East-West straight and right turn for 26 seconds, Phase 2 for an East-West left turn for 26 seconds, Phase 3 for a North-South straight and right turn for 25 seconds, and Phase 4 for a North-South left turn for

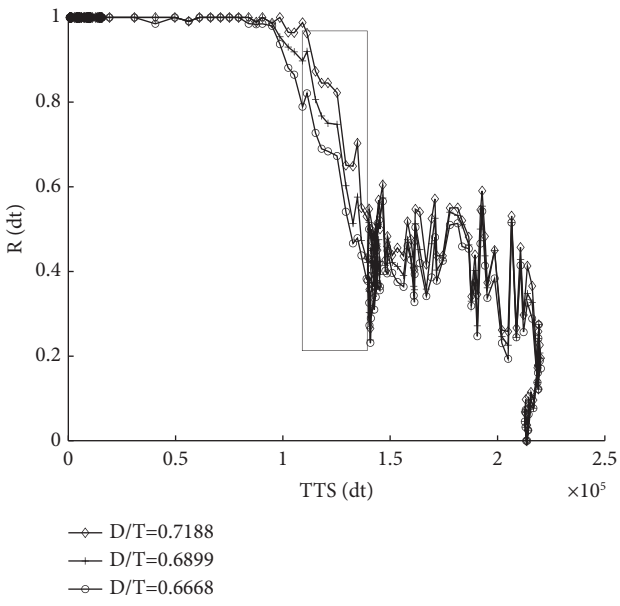

Figure 7: Trend chart of reliability truth value under different delay travel time ratio thresholds of the simulated road network.

Table 4: Values of parameters for reliability estimation model.

Estimation model parameter	Parameter value
Parameters of the BPR function α	0.132
Parameters of the BPR function β	1.543
Coefficient for free-flow variance estimation δ_f	$5.13E-03$
The coefficient for saturation variance estimation δ_s	$1.08E-03$
The coefficient for congestion variance estimation δ_j	$2.43E-03$

25 seconds. A 3-second yellow time and a 2-second all-red time are allocated between each signal phase to clear the intersection from vehicles and prevent congestion. The signal cycle time for each intersection is set at 120 seconds.

To ensure unbiased experimental results and account for variations in vehicle inputs on different roads, each road segment has a consistent traffic volume of 2000 passenger car units per hour (pcu/h). Traffic is made up of 91% passenger cars, 3% large trucks, and 6% buses. To maintain a safe and efficient flow of traffic, expected speeds are set at 50 km/h for passenger cars, 40 km/h for large trucks, and 30 km/h for buses.

In order to study the influence of different detector deployment schemes on the accuracy of road network TTR, five detector distribution schemes have been set up. These schemes consider the comprehensiveness and density of detector placements in the road network to assess TTR. Specific detector deployment schemes are as follows:

Five different detector deployment schemes are presented in Figure 9. The first scheme places a detector on each link in the east-west direction, but not on any north-south links. These detectors monitor vehicle data within 500 meters of deployed links. The second scheme also places a detector on each link, but removes the four detectors on the lower right square of the network. The third scheme places a detector on each link throughout the network, monitoring vehicle data within 500 meters. The fourth scheme places two detectors on each link throughout the network, monitoring vehicle data within 250 meters. The fifth and final scheme places three detectors on each link throughout the network, monitoring vehicle data within 167 meters. Through simulation experiments, Table 6 shows a comparison between estimated TTR values and ground truth values for different schemes, as well as the impact of detector deployment on estimation accuracy.

To reflect the sparsity of the data, the original data were randomly screened with penetration rates of 5%, 10%, and 20%, respectively. After applying the same data processing methods as the original data, the estimated TTR values and actual values for the five detector deployment schemes were obtained. The obtained results of the TTR estimation and actual values are presented in Table 7.

To visually depict disparities between original TTR and post-random screening reliability (at penetration rates of 5%, 10%, and 20%), we assessed the effects of detector deployment on accuracy and reliability fluctuations. The findings, regarding accuracy impact and reliability shifts following penetration screening, are detailed in Tables 8 and 9.

Table 8 reveals that post random screening at penetration rates of 5%, 10%, and 20%, TTR data trends are generally aligned with the original data. Notably, under Scheme 5, the estimated reliability values are closest to the actual values, indicating minimal impact on the estimation accuracy of this detector scheme.

Table 9 illustrates that, notwithstanding the variations between actual and estimated reliability values, the estimations exhibit consistency subsequent to penetration screening under diverse schemes. The simulated network data reasonably reflect the accuracy of the simulation results.

Conclusively, the data analysis and scheme evaluation underscore that detector deployment uniformity, completeness, and density influence reliability estimation accuracy. Enhanced uniform, complete, and dense deployment leads to more accurate TTR estimation.

4.3. Analysis of the Effectiveness of the T-TTR Method. In this subsection, simulation experiments were conducted using a minimal road network unit consisting of a 3×3 grid. Specific data for simulated road networks remain consistent with Section 4.1. Within VISSIM, nine nodes were chosen to define the road network region, and region numbers were assigned sequentially from top to bottom and left to right, ranging from 1 to 9. The selected road network nodes and their corresponding numbers are depicted in Figure 10.

Each node is designated to represent a small road network. The travel time of each vehicle within the road network is represented by the difference between its end time and start time. Time windows are established based on the start time of the vehicle, with a total of 10,800 seconds divided into 12 windows of 900 seconds each.

Assuming uniform signal timings for the nine intersections, the vehicle composition is exclusively passenger cars, and the traffic flow input adheres to the daily traffic volume variation pattern of the network. Sudden incidents are disregarded, and the delay of each vehicle within a node is considered the delay within the small road network. By calculating the ratio of delay to travel time for each vehicle, the reliability of individual vehicles is determined. The count of vehicles with reliability values equal to or below the threshold indicates the number of vehicles with reliable travel within the road network. Dividing the count of reliable vehicles by the total number of vehicles within each node yields the TTR of that node (small road network). The acquired TTRs for diverse time windows across various road network regions are presented in Table 10.

The 80% rule advises that substances with a nonmissing portion constituting less than 80% of the total sample should be excluded. Adhering to this principle, the experiment in this subsection employs a 20% penetration rate, assuming that the count of road network regions with missing data is no more than 2. Employing the proposed T-TTR estimation method on sparse data yields TTRs for distinct road network regions, as summarized in Table 11.

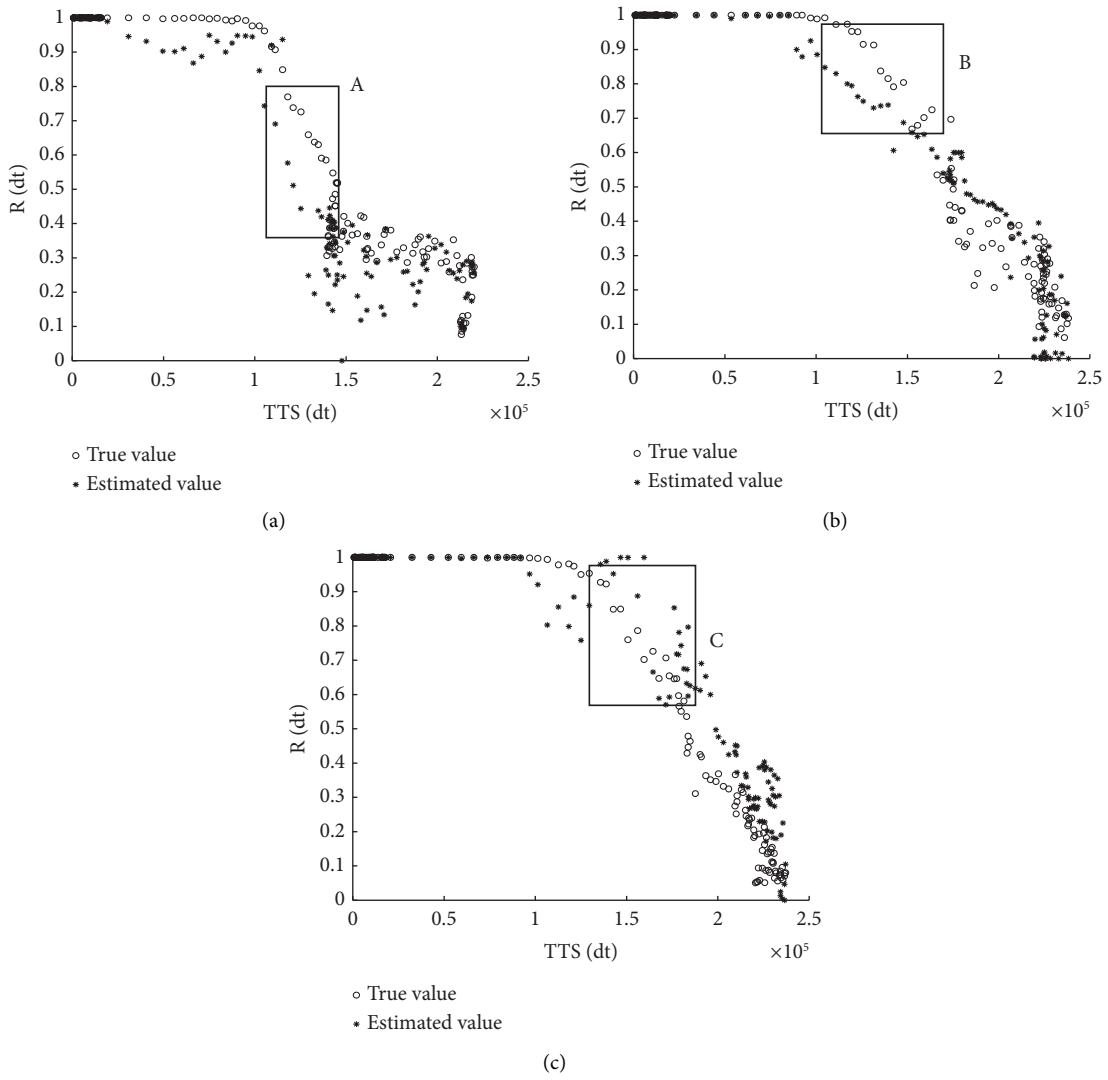

Figure 8: Comparison chart of TTS and reliability true values and estimated values. (a) Depicts a signal cycle length of 60 seconds; (b) depicts a signal cycle length of 90 seconds; (c) depicts a signal cycle length of 120 seconds.

Table 5: Values of parameters for reliability estimation model.

Signal cycle length (s)	Mean error	Mean absolute error
60	−0.0451	0.0568
90	−0.0143	0.0617
120	0.0577	0.0759

From the 6th to the 12th time window, comprehensive data imputation results in an average error of 0.0059, clearly demonstrating the effectiveness of the T-TTR method in accurately estimating road network TTR.

4.4. Analysis of the Applicability of the T-TTR Method. This subsection conducts a case study to analyze the estimation results of the T-TTR method at various data penetration rates and discusses the impact of data sparsity on the estimation technique. We employs simulated sparse trajectory data from VISSIM traffic data. Realistically, vehicle data collection across different road network regions is often uneven. Four comparison groups based on data uniformity, are proposed as follows:

Control Group: Uniform data removal from VISSIM data. A certain percentage of VISSIM data is uniformly removed, resulting in a specified penetration rate (e.g., 80% data removal for a 20% penetration rate).

Experimental Group 1: Random data removal from VISSIM data. Non-uniform data removal is employed to simulate random data gaps.

Experimental Group 2: Road network reliability estimated using the HaLRTC method. Tensor completion is applied to randomly missing data using the HaLRTC estimation method.

Experimental Group 3: Building upon Experimental Group 2 data, data from a specific road network region meeting defined criteria are treated as missing data with a value of 0. Tensor completion is then performed using the T-TTR estimation method.

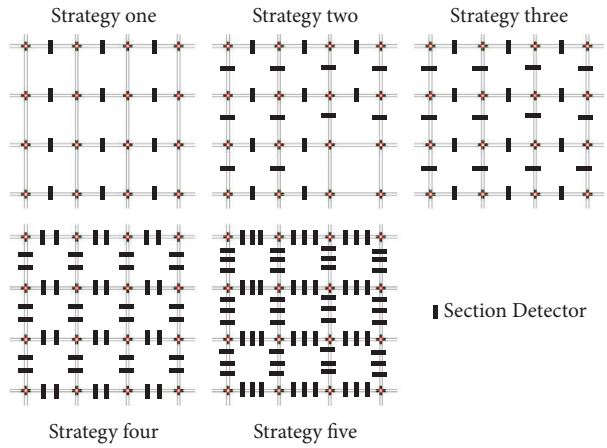

Figure 9: Detector deployment strategies.

Table 6: Comparison of estimated and true road network TTR for different schemes.

Scheme	TTR (%)	Impact on accuracy (%)
True value	44.37	—
Scheme 1	41.68	−2.690
Scheme 2	40.90	−3.470
Scheme 3	42.19	−2.180
Scheme 4	44.43	0.060
Scheme 5	45.62	1.250

Table 7: Estimations of TTR for various schemes under penetration rate screening.

Scheme	Penetration rate 5 (%)	Penetration rate 10 (%)	Penetration rate 20 (%)
True value	47.70	48.36	46.13
Scheme 1	42.47	41.68	41.68
Scheme 2	40.52	41.29	40.90
Scheme 3	40.90	40.52	40.52
Scheme 4	43.64	43.25	43.64
Scheme 5	45.22	45.62	45.22

Table 8: Effect of TTR accuracy under penetration rates of 5%, 10%, and 20%.

Strategy	Origin data (%)	Penetration rate 5 (%)	Penetration rate 10 (%)	Penetration rate 20 (%)
Scheme 1	−2.690	−5.227	−6.675	−4.455
Scheme 2	−3.470	−7.177	−7.065	−5.235
Scheme 3	−2.180	−6.797	−7.835	−5.615
Scheme 4	0.060	−4.057	−5.105	−2.495
Scheme 5	1.250	−2.477	−2.735	−0.915

Considering the limited availability of real-world trajectory data, typically exhibiting low penetration rates, representations are made for 5%, 10%, and 20% data penetration rates. Table 12 presents the accuracy of road network reliability obtained by the three methods across varying penetration rates.

Table 12 presents findings from a uniform data analysis, indicating that different penetration rates yield varying results among Experimental Groups 1, 2, and 3. Notably, Experimental Group 3 and 2 outperformed Group 1, while the Control Group exhibits the lowest values. Remarkably, Experimental Group 3, applying the T-TTR estimation method, displays heightened precision as the penetration rate rises. At 5% penetration rate, Experimental Groups 3 and 2 exhibit comparable accuracy. This underscores that a more uniform data distribution within the road network enhances the fidelity of TTR to actual conditions. The proposed T-TTR

Table 9: Variability in TTR under penetration rates of 5%, 10%, and 20%.

Strategy	Penetration rate 5 (%)	Penetration rate 10 (%)	Penetration rate 20 (%)
True value	3.33	3.99	1.77
Scheme 1	0.79	0.00	0.00
Scheme 2	−0.38	0.39	0.00
Scheme 3	−1.29	−1.67	−1.67
Scheme 4	−0.79	−1.18	−0.79
Scheme 5	−0.40	0.00	−0.40

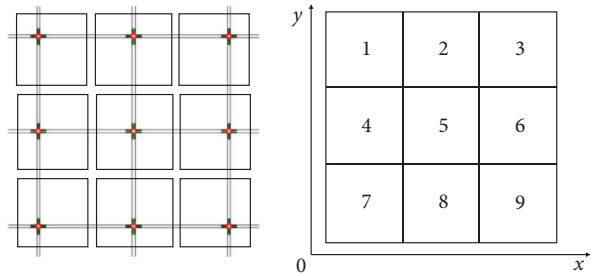

Figure 10: Diagram of road network nodes and network IDs.

Table 10: TTR in road network regions under complete data.

Time window	TTR		
1: 0–900	1	1	1
	1	1	1
	1	1	1
2: 900–1800	1	1	1
	1	1	1
	1	1	1
3: 1800–2700	1	1	1
	1	1	1
	1	1	1
4: 2700–3600	1	1	1
	1	1	1
	1	1	1
5: 3600–4500	1	1	1
	1	1	1
	1	1	1
6: 4500–5400	0.9288	0.9171	0.9300
	0.9324	0.7987	0.8687
	0.9034	0.9314	0.9381
7: 5400–6300	0.5955	0.2896	0.6978
	0.6173	0.2447	0.4272
	0.9254	0.7488	0.8868
8: 6300–7200	0.5463	0.3229	0.4568
	0.5429	0.0556	0.1374
	0.4898	0.7135	0.7258
9: 7200–8100	0.4373	0.1691	0.3327
	0.5837	0.2921	0.2611
	0.6651	0.4840	0.3970
10: 8100–9000	0.4654	0.1360	0.2013
	0.7017	0.4640	0.4028
	0.6675	0.5660	0.2625
11: 9000–9900	0.4749	0.1469	0.1418
	0.5518	0.3757	0.4218
	0.3434	0.5333	0.2222
12: 9900–10800	0.1976	0.1766	0.2565
	0.3046	0.2561	0.2042
	0.2926	0.3710	0.1412

Table 11: TTR in road network regions with 20% penetration rate sparse data.

Time window	TTR		
1: 0–900	1	1	1
	1	1	1
	1	1	1
2: 900–1800	1	1	1
	1	1	1
	1	1	1
3: 1800–2700	1	1	1
	1	1	1
	1	1	1
4: 2700–3600	1	1	1
	1	1	1
	1	1	1
5: 3600–4500	1	1	1
	1	1	1
	1	1	1
6: 4500–5400	0.9430	0.9182	0.9222
	0.9053	0.7923	0.8827
	0.9176	0.9398	0.9381
7: 5400–6300	0.6243	0.2651	0.7043
	0.5843	0.2353	0.4611
	0.5897	0.7389	0.8529
8: 6300–7200	0.5629	0.2911	0.4233
	0.5318	0.0313	0.1418
	0.4514	0.6596	0.7973
9: 7200–8100	0.3788	0.2190	0.3421
	0.6400	0.2636	0.2062
	0.5840	0.4957	0.3830
10: 8100–9000	0.5042	0.1284	0.1750
	0.7273	0.3258	0.4712
	0.6310	0.5581	0.3226
11: 9000–9900	0.4561	0.1778	0.0787
	0.5325	0.3377	0.4028
	0.3617	0.5373	0.1667
12: 9900–10800	0.2727	0.1857	0.3171
	0.3333	0.2468	0.2500
	0.2838	0.3146	0.1200

Table 12: Analysis of different experimental groups with different penetration rates.

RMSE	Control group	Experimental group 1	Experimental group 2	Experimental group 3
Penetration rate 20%	0.0441	0.3222	0.1285	0.1128
Penetration rate 10%	0.0480	0.2205	0.1332	0.1172
Penetration rate 5%	0.0885	0.3019	0.1170	0.1223
MAE	Control group	Experimental group 1	Experimental group 2	Experimental group 3
Penetration rate 20%	0.0229	0.1842	0.0546	0.0480
Penetration rate 10%	0.0953	0.0953	0.0750	0.0647
Penetration rate 5%	0.0275	0.1650	0.0692	0.0691

method excels particularly when penetration rates surpass 5%.

For assessing the influence of data penetration on the T-TTR method, Figure 11 illustrates the ground truth and chromaticity maps of road network TTR at 5%, 10%, and 20% penetration rates. Red hues indicate heightened congestion, with reliability close to 0 denoting severe congestion. The figure demonstrates escalating congestion as time windows extend. The value trend of the T-TTR method aligns with the ground truth, confirming its effectiveness. Analyzing the influence of different penetration rates on the T-TTR method, the errors for penetration rates of 5%, 10%, and 20% are calculated and summarized in Table 13 for error analysis.

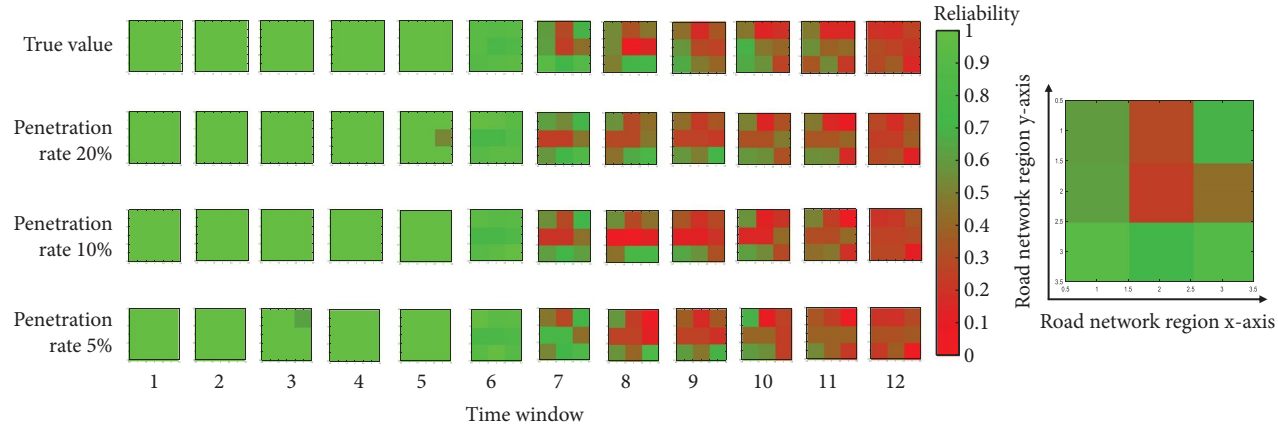

Figure 11: Road network TTR at different penetration rates using the T-TTR estimation method.

Table 13: Errors of T-TTR estimation method at different penetration rates.

	Penetration rate 5%	Penetration rate 10%	Penetration rate 20%
RMSE	0.1223	0.1172	0.1128
MAE	0.0691	0.0647	0.0580

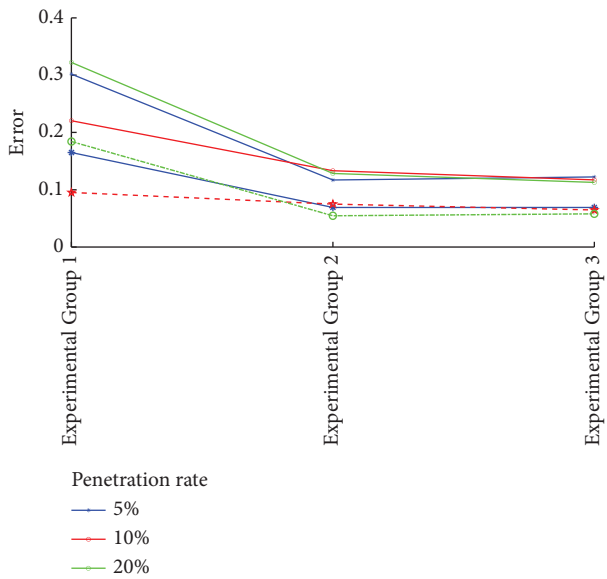

Figure 12: Errors for different experimental groups at various penetration rates.

Table 13 demonstrates a clear relationship: higher penetration rates result in more accurate road network TTR values from the T-TTR estimation method. Figure 12 presents a comprehensive comparison of Experimental Groups 1, 2, and 3 with penetration rates of 5%, 10%, and 20%. The graph confirms that, at the same penetration rate, the T-TTR method consistently outperforms Experimental Groups 1 and 2, showcasing superior accuracy. Moreover, higher penetration rates within each group yield enhanced accuracy. This underscores that in practical scenarios, higher GPS coverage and richer vehicle trajectory data yield more precise estimations of road network TTR. Incorporating enhancements of the T-TTR method over HaLRTC yields smaller errors, affirming the utility of spatiotemporal correlations. Consequently, the T-TTR method excels in estimating road network TTR compared to the HaLRTC method.

5. Conclusion

This study defines road network TTR as the likelihood that the ratio of delay to travel time for all vehicles in the network is below a specified threshold. Utilizing road network and vehicle data from Huangpu District of Shanghai over four days, the study confirms that the delay-to-travel time ratio follows a normal distribution. Building on this, the study presents a calculation method for road network TTR and outlines parameter setting strategies. Given the normal distribution of delay-to-travel time ratios, study introduces the S-TTR and T-TTR estimation methods. Simulation experiments yield the following insights:

(i) The S-TTR estimation method accurately gauges road network TTR using only partial traffic data. It captures reliability fluctuations effectively, particularly when network traffic is not saturated.

(ii) The nonuniform and incomplete deployment of detectors leads to a reduction in the precision of the S-TTR method, while the uniform and comprehensive deployment of detectors contributes to an enhancement in estimation accuracy.

(iii) The T-TTR method, rooted in tensor completion theory, is contrasted with the spatially and temporally optimized HaLRTC algorithm. T-TTR effectively fills gaps in data with high precision.

Data uniformity enhances road network TTR accuracy. The T-TTR method is notably more accurate when penetration rates surpass 5%, yielding more precise outcomes.

This study does not account for adaptive signal control or traffic guidance effects on road network TTR. Future research aims to address these limitations by integrating

crowd-sourced vehicle trajectory data to enhance the research method, achieving more precise road network TTR estimation through data fusion from a wider range of sources.

Data Availability

All the data used to support the findings of this study are included within the paper.

Conflicts of Interest

The authors declare that they have no conflicts of interest.

Acknowledgments

This work was financially supported by the National Natural Science Foundation of China under Grants no. 52102398 and by the Science and Technology Commission of Shanghai Municipality under Grants no. 23692107600.

References

[1] R. Saedi, M. Saeedmanesh, A. Zockaie, M. Saberi, N. Geroliminis, and H. S. Mahmassani, "Estimating network travel time reliability with network partitioning," *Transportation Research Part C: Emerging Technologies*, vol. 112, pp. 46–61, 2020.

[2] E. Jenelius, "Public transport experienced service reliability: integrating travel time and travel conditions," *Transportation Research Part A: Policy and Practice*, vol. 117, pp. 275–291, 2018.

[3] Z. Yang, X. Li, Y. Guo, and X. Qian, "Understanding active transportation accessibility's impacts on polycentric and monocentric cities' housing price," *Research in Transportation Economics*, vol. 98, Article ID 101282, 2023.

[4] Y. Guo, X. Qian, T. Lei, S. Guo, and L. Gong, "Modeling the preference of electric shared mobility drivers in choosing charging stations," *Transportation Research Part D: Transport and Environment*, vol. 110, Article ID 103399, 2022.

[5] S.-K. S. Fan, C.-J. Su, H.-T. Nien, P.-F. Tsai, and C.-Y. Cheng, "Using machine learning and big data approaches to predict travel time based on historical and real-time data from Taiwan electronic toll collection," *Soft Computing*, vol. 22, no. 17, pp. 5707–5718, 2018.

[6] I. Sanaullah, M. Quddus, and M. Enoch, "Developing travel time estimation methods using sparse GPS data," *Journal of Intelligent Transportation Systems*, vol. 20, no. 6, pp. 532–544, 2016.

[7] F. F. Zheng and H. Van Zuylen, "The development and calibration of a model for urban travel time distributions," *Journal of Intelligent Transportation Systems*, vol. 18, no. 1, pp. 81–94, 2014.

[8] L. Bellocchi and N. Geroliminis, "Unraveling reaction-diffusion-like dynamics in urban congestion propagation: insights from a large-scale road network," *Scientific Reports*, vol. 10, no. 1, p. 4876, 2020.

[9] A. Khani and S. D. Boyles, "An exact algorithm for the mean-standard deviation shortest path problem," *Transportation Research Part B: Methodological*, vol. 81, pp. 252–266, 2015.

[10] M. A. P. Taylor, "Fosgerau's travel time reliability ratio and the Burr distribution," *Transportation Research Part B: Methodological*, vol. 97, pp. 50–63, 2017.

[11] H. P. Li, F. He, X. Lin, Y. H. Wang, and M. Li, "Travel time reliability measure based on predictability using the Lempel-Ziv algorithm," *Transportation Research Part C: Emerging Technologies*, vol. 101, pp. 161–180, 2019.

[12] F. N. Yang, G. L. Liu, L. P. Huang, and C. S. Chin, "Tensor decomposition for spatial-temporal traffic flow prediction with sparse data," *Sensors*, vol. 20, no. 21, p. 6046, 2020.

[13] L. Lin, J. X. Li, F. Chen, J. P. Ye, and J. P. Huai, "Road traffic speed prediction: a probabilistic model fusing multi-source data," *IEEE Transactions on Knowledge and Data Engineering*, vol. 30, no. 7, pp. 1310–1323, 2018.

[14] K. Tang, S. Y. Chen, and Z. Y. Liu, "Citywide spatial-temporal travel time estimation using big and sparse trajectories," *IEEE Transactions on Intelligent Transportation Systems*, vol. 19, no. 12, pp. 4023–4034, 2018.

[15] H. Zhong, G. Q. Qi, W. Guan, and X. C. Hua, "Application of nonnegative tensor factorization for intercity rail-air transport supply configuration pattern recognition," *Sustainability*, vol. 11, no. 6, p. 1803, 2019.

[16] G. Pastor, "A low-rank tensor model for imputation of missing vehicular traffic volume," *IEEE Transactions on Vehicular Technology*, vol. 67, no. 9, pp. 8934–8938, 2018.

[17] H. Tan, G. Feng, J. Feng, W. Wang, Y.-J. Zhang, and F. Li, "A tensor-based method for missing traffic data completion," *Transportation Research Part C: Emerging Technologies*, vol. 28, pp. 15–27, 2013.

[18] Y. H. U. Z. C. A. I. Dian-hai Wang, "Dynamic road resistance model of intermittent flow on urban roads based on BPR function," *Journal of Jilin University (Engineering and Technology Edition)*, vol. 53, no. 7, pp. 1951–1961, 2023.

[19] F. Zhao, L. Fu, M. Zhong et al., "Development and validation of improved impedance functions for roads with mixed traffic using taxi GPS trajectory data and simulation," *Journal of Advanced Transportation*, vol. 2020, Article ID 7523423, 12 pages, 2020.

[20] Y. Li, R. Mohajerpoor, and M. Ramezani, "Perimeter control with real-time location-varying cordon," *Transportation Research Part B: Methodological*, vol. 150, pp. 101–120, 2021.

[21] V. L. Knoop, H. van Lint, and S. P. Hoogendoorn, "Traffic dynamics: its impact on the macroscopic fundamental diagram," *Physica A: Statistical Mechanics and Its Applications*, vol. 438, pp. 236–250, 2015.

[22] J. W. Wang, X. Z. He, S. Peeta, and X. G. Yang, "Feedback perimeter control with online estimation of maximum throughput for an incident-affected road network," *Journal of Intelligent Transportation Systems*, vol. 26, no. 1, pp. 81–99, 2022.

[23] L. Y. Zheng and B. Wu, "A reinforcement learning based traffic control strategy in a macroscopic fundamental diagram region," *Journal of Advanced Transportation*, vol. 2022, Article ID 5681234, 12 pages, 2022.

[24] J. Liu, P. Musialski, P. Wonka, and J. Ye, "Tensor completion for estimating missing values in visual data," *IEEE Transactions on Pattern Analysis and Machine Intelligence*, vol. 35, no. 1, pp. 208–220, 2013.